HHS Public Access

Author manuscript

Adv Mater. Author manuscript; available in PMC 2018 April 01.

Published in final edited form as:

Adv Mater. 2017 April ; 29(16): . doi:10.1002/adma.201606209.

Erythrocyte-Platelet Hybrid Membrane Coating for Enhanced Nanoparticle Functionalization

Diana Dehaini, **Xiaoli Wei**, **Ronnie H. Fang**, **Sarah Masson**, **Pavimol Angsantikul**, **Brian T. Luk**, **Yue Zhang**, **Man Ying**, **Yao Jiang**, **Ashley V. Kroll**, **Weiwei Gao**, and **Liangfang Zhang***

Department of NanoEngineering and Moores Cancer Center, University of California, San Diego, La Jolla, CA 92093, U.S.A

Table of content entry

Biomimetic dual membrane-functionalized nanoparticles, incorporating the natural properties of two different cell types, are fabricated by a facile process employing fused cell membranes. The resulting hybrid cell membrane-coated nanoparticles retain protein markers from each source cell and combine the unique functions of both. The reported approach opens the door for the fabrication of biocompatible nanocarriers with increasingly complex functionality.

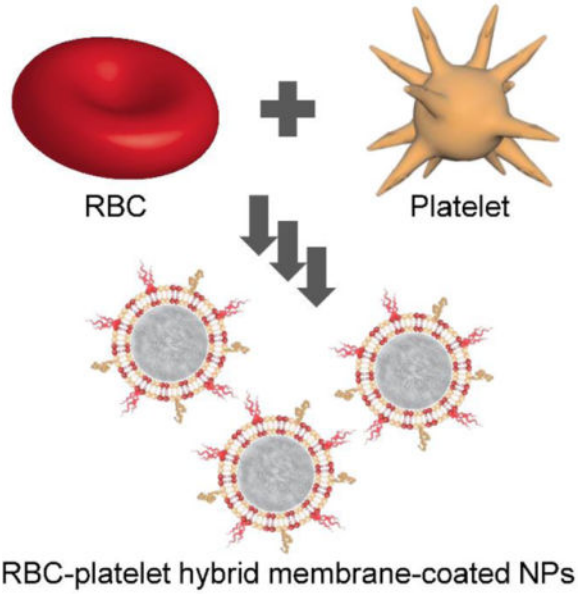

Keywords

nanomedicine; biomimetic nanoparticle; membrane fusion; long circulation; targeted delivery

Nanotechnology has increasingly been employed for the design of drug delivery and imaging modalities in order to further improve efficacy in the clinic. There are many classes of nanoscale delivery vehicles, including liposomes, polymeric nanoparticles, and inorganic

zhang@ucsd.edu, Tel: +1-858-246-0999.

systems among many others.[1–4] For applications such as cancer treatment, the use of such nanoparticle platforms has the potential to enable greatly enhanced potency while minimizing the systemic toxicity associated with traditional therapeutics.[5–9] Recently, a new class of drug nanocarrier has been reported that is fabricated by combining synthetic nanoparticulate cores with a biologically derived membrane coating.[10–13] These biomimetic, cell membrane-coated nanoparticles directly leverage the versatility and complexity of cellular membrane, which has been crafted by nature through the process of evolution to perform specific functions, especially with regards to biointerfacing.[14–17] By translocating the entire membrane from a cell onto the surface of a nanoparticle, all biologically relevant surface moieties are transferred, including those that can potentially be used for immune evasion and targeting, two highly desirable properties. Additionally, it may be possible to take advantage of cell-specific functionalities that are known to exist, but have not been well characterized on a fundamental biological level.[18–20]

The first platform of this type employed red blood cells (RBCs), also known as erythrocytes, as the source material in order to achieve lengthened blood residency, and the resulting RBC membrane-coated nanoparticles (RBCNPs) displayed significantly enhanced circulation half-lives compared with a nanoparticle stabilized by a layer of polyethylene glycol (PEG).[21] It was later demonstrated that these cell membrane-coated nanoparticles exhibited right-side-out membrane orientation and included immunomodulatory markers such as CD47 at the same density as the original RBCs.[22] RBCNPs have also been used for novel detoxification applications, including for toxic nerve agents and bacterial toxins.[23–26] More recently, many different cell types other than RBCs, including platelets, white blood cells, cancer cells, stem cells, and even bacteria, have been used to source the membrane material, each with its own set of unique characteristics.[14,18,27–29] Of note, expansion of the cell membrane-coated platform to other cells has enabled the fabrication of naturally targeted drug carriers.[30] This includes the use of cancer cells for homotypic delivery to the tumor of origin, or platelets, which play a role in a wide array of different diseases that range from atherosclerosis to bacterial infection.

While cell membrane coating is a powerful method of enhancing nanoparticle utility, it is often desirable to introduce additional functionality depending on the specific application. For example, while RBCNPs can circulate for extended periods of time, the addition of a targeting ligand can help to improve localization to the desired target, such as a tumor.[31] Herein, we report on an approach for increasing the number of functions that can be performed by a single membrane-coated nanocarrier *via* the simultaneous derivation of functionality from multiple cell types. This novel approach, which involves the fusion of natural cell membranes from different origins, represents a facile and effective means of fashioning nanoparticles that can perform increasingly complex tasks within biologically relevant contexts. Specifically, we aimed to combine the functionality of human-derived RBCs and platelets (Figure 1A). The resulting RBC-platelet hybrid membrane-coated nanoparticles ([RBC-P]NPs) were thoroughly characterized, and it was demonstrated that they retained functionality that is characteristic of each individual cell type. Finally, we show that these dual membrane-coated nanoparticles displayed *in vivo* properties consistent with expectations, warranting further study.

In order to fabricate the [RBC-P]NPs, the first step was to verify that it was possible to fuse RBC membrane and platelet membrane together, the product of which would then be used as the base material for downstream nanoparticle preparation. To test for fusion, platelet membrane was doped with two different dyes that constituted a Förster resonance energy transfer (FRET) pair and added to increasing amounts of RBC membrane under elevated temperature and stirring (Figure 1B). It was observed that, as the amount of RBC material increased, there was a recovery of fluorescence at the lower emission wavelength around 534 nm, indicating the interspersing of the two membrane materials weakening the FRET interactions in the original platelet membrane. Using a 1:1 protein weight ratio of RBC membrane to platelet membrane for further study, we fabricated a batch of the hybrid [RBC-P]NPs. RBC membrane labeled with a red fluorescent dye was fused with platelet membrane that was labeled with a green fluorescent dye, and the resultant material was coated onto preformed poly(lactic-*co*-glycolic acid) (PLGA) cores. When a dilute solution of the [RBC-P]NPs was immobilized in glycerol and viewed under confocal microscopy, significant colocalization of fluorescent signals was observed (Figure 1C). In stark contrast, a mixture of RBCNPs and platelet membrane-coated nanoparticles (PNPs) fabricated with the individual fluorescently labeled membranes exhibited distinct red and green punctates. It was further demonstrated that the RBC and platelet membranes were retained on the [RBC-P]NPs at a ratio nearly identical to the 1:1 input (Figure 1D). The results indicate that it was indeed possible to fuse the two types of natural cell membrane and incorporate the material of both onto the same nanoparticle.

Dynamic light scattering (DLS) was used to compare the [RBC-P]NPs with each single membrane formulation of RBCNPs or PNPs (Figure 2A,B). It was observed that bare PLGA cores, which were originally 80 nm in size, exhibited a very uniform increase in size of approximately 20 nm after coating with each membrane. Additionally, the surface zeta potential increased by over 10 mV for each of the three nanoparticle types compared with PLGA cores, approaching the value of approximately −25 mV observed for each of the different membrane vesicles. This phenomenon is commonly seen after membrane coating and indicates shielding of the highly negative cores with the less negative outer membrane surface.[14,21] When visualized under transmission electron microscopy (TEM), the RBCNPs, PNPs, and hybrid [RBC-P]NPs all displayed a characteristic core-shell structure that was consistent with the sizing results (Figure 2C). A set of assays were then carried out to assess nanoparticle stability in various media. To determine stability of the hybrid formulation in solution over time, samples were stored in either water or 1× phosphate buffered saline (PBS, pH 7.4) and the size was measured over time (Figure 3A,B). The [RBC-P]NPs, in addition to RBCNPs and PNPs, exhibited stable size over the 3 week duration of the study in both solutions. In contrast, bare PLGA cores, which are only stabilized by charge repulsion, immediately aggregated in PBS to the micron range. Additionally, [RBC-P]NPs displayed little change in absorbance before and after incubation with 100% serum, while bare PLGA cores again exhibited a large increase (Figure 3C). Regarding long-term storage, the [RBC-P]NP formulation exhibited near identical size both before freeze-drying and after resuspension (Figure 3D). Taken together, the characterization data give strong physical evidence for successful coating by the fused membrane material,

with results in line with what would be expected given the properties of the single membrane-coated RBCNPs and PNPs.

To analyze the overall protein content of the [RBC-P]NPs, SDS-PAGE was used to run RBC membrane, platelet membrane, hybrid membrane, and all corresponding nanoparticle formulations followed by Coomassie staining for visualization (Figure 4A). Compared with RBCNPs and PNPs, the [RBC-P]NPs had a profile that represented the union of the two single membrane formulations. As expected, all nanoparticles had protein profiles that largely mirrored that of the corresponding membrane. To analyze specific protein markers, western blotting analysis was carried out (Figure 4B). CD235a, a major RBC sialoglycoprotein also known as glycophorin A,[32] as well as the blood group A antigen, were present on RBCNPs and also to a lesser degree on [RBC-P]NPs. CD41 and CD61, which collectively form integrin αIIbβ3,[33] are important for platelet adhesion as well as activation, and both were present on PNPs and also to a lesser degree on [RBC-P]NPs. Meanwhile, CD47,[34,35] an immunomodulatory protein responsible for inhibiting macrophage uptake that is expressed by both cell types, was found at a near equivalent degree on RBCNPs, PNPs, and [RBC-P]NPs. Additionally, immunogold staining followed by TEM imaging provided visual evidence that a single [RBC-P]NP could simultaneously present both RBC-specific and platelet-specific markers (Figure 4C). Ultimately, the protein analysis carried out here indicates that functionalization with the fusion membrane can bestow both RBC and platelet surface proteins onto the hybrid [RBC-P]NPs, although the exact nature of the intraparticle distribution of individual protein markers at the molecular level remains unknown.

Upon confirming successful transference of markers unique to both source cells, we next sought to characterize the hybrid membrane coating on a functional level. Both RBCNPs and PNPs, given the presence of immunomodulatory markers on their surface, have been shown to be adept at minimizing macrophage uptake.[14,22,36] An uptake study using human THP-1 monocytes differentiated into macrophage-like cells was thus carried out to evaluate this property in [RBC-P]NPs (Figure 5A). Using flow cytometric analysis after incubation with the macrophage-like cells, [RBC-P]NPs had low uptake consistent with both RBCNPs and PNPs, whereas PLGA cores, without immunomodulatory membrane coatings, exhibited a high degree of uptake. As an RBC-specific functional marker, we next assessed the level of acetylcholinesterase activity (Figure 5B). The enzyme is important for regulating neurotransmitter concentrations, and RBCNPs have been shown to be potent decoys capable of neutralizing lethal doses of poisonous compounds that can deactivate the protein.[25] It was confirmed that [RBC-P]NPs had an intermediate level of activity compared with RBCNPs and PNPs, the latter of which had a negligible amount of activity. This was further reflected in detoxification capacity, as the amount of dichlorvos, a model organophosphate, left in solution after incubation with each nanoformulation was inversely related to acetylcholinesterase activity (Figure 5C). Regarding platelet-specific functionality, the cancer targeting properties of the hybrid [RBC-P]NPs was first evaluated. PNPs, given the large number of disease-relevant binding markers present on their surface, have been shown to be effective at targeting certain metastatic cancers.[37] Using both flow cytometry as well as fluorescent imaging, it was demonstrated that [RBC-P]NPs bound to highly metastatic MDA-MB-231 human breast cancer cells within the spectrum between RBCNPs and PNPs,

which exhibited low and high amounts of binding, respectively (Figure 5D,E). On the other hand, normal HFF-1 human foreskin fibroblasts showed significantly lowered binding by all nanoparticle types (Figure 5D), and this was further confirmed by a co-culture imaging study using [RBC-P]NPs (Figure 5F). After binding to cancer cells, it is expected that the hybrid nanoparticles would be endocytosed via the clathrin-dependent pathway.[37] To assess *in vivo* targeting ability, a mouse model of atherosclerosis, which platelets are known to interact with, was employed. Fluorescence imaging of aortas collected after intravenous nanoparticle administration revealed a trend consistent to what was observed for the *in vitro* studies (Figure 5G). Overall, the ability of [RBC-P]NPs to incorporate the functional properties of both RBCs and platelets is encouraging and provides a strong indication that other cell-specific functions should likewise be present on the dual membrane-coated nanoparticles.

Finally, to evaluate the [RBC-P]NP formulation for potential *in vivo* application, the circulation and biodistribution of the nanoparticles were evaluated using a mouse model. Murine-derived RBCs and platelets, along with fluorescently labeled PLGA cores, were used as the starting materials to fabricate RBCNPs, PNPs, and [RBC-P]NPs. To test the circulation half-life, nanoparticles were administered intravenously via the tail vein, and blood was sampled at increasing timepoints to evaluate remaining nanoparticle concentration (Figure 6A). After fitting to a two-phase decay model, it was apparent that all three formulations exhibited very similar circulation profiles. Indeed, both RBCNPs and PNPs have previously been reported to circulate for extended periods of time upon administration.[21,37] Numerical analysis indicated that RBCNPs, PNPs, and [RBC-P]NPs had one-phase half-lives of 5.7, 5.7, and 6.4 hours and two-phase elimination half-lives of 42.4, 38.3, and 51.8 hours, respectively. All values were within error of each other (see Experimental Section). To analyze biodistribution, nanoparticles were again administered intravenously, and the mice were euthanized 24 hours afterwards in order to collect the heart, lungs, kidneys, liver, and spleen for fluorescence analysis (Figure 6B). All three nanoformulations, including the [RBC-P]NPs, displayed similar organ-level localization, with the majority of the nanoparticles found in the liver and spleen as a result of reticuloendothelial uptake. This pattern is consistent with what has been previously reported for similar nanoformulations.[14,21] The uniformity in circulation and distribution profiles between all experimental groups can likely be explained by the fact that, under normal conditions, both RBCs and platelets are inherently designed to persist in the bloodstream for extended periods of time; in healthy individuals, there is an absence of reactive substrates and molecules that can contribute to accelerated clearance of either cell type.

In conclusion, we have successfully fabricated a new class of cell membrane-coated nanocarrier that combines the function of two different cell types. It was confirmed that it is possible to fuse RBC membrane and platelet membrane together, using it as a coating material to fabricate hybrid [RBC-P]NPs. Physically, the resultant particles were similar to pure, single membrane formulations of either RBCNPs or PNPs. On a protein and functional level, the [RBC-P]NPs represented a cross between the two parent nanoparticle types, retaining properties once only exclusive to either. The reported method of bestowing nanoparticles with enhanced functionality provides a facile and natural alternative to synthetic post-functionalization strategies. Importantly, the dual membrane-coated

nanoparticles are expected to maintain excellent biocompatibility as long as the source cell types are appropriately chosen. This approach can also potentially be used to marry functions across disparate fields, including targeted drug delivery, immune modulation, and detoxification. It can easily be envisioned that a countless number of different combinations can be explored, and this may ultimately give rise to new multi-membrane nanoparticle platforms that have the potential to outperform their single membrane counterparts.

Experimental Section

Membrane Fusion Study

Human RBC membrane was derived from whole blood (BioreclamationIVT) and human platelet membrane was derived from platelet-rich plasma (San Diego Blood Bank) using previously described protocols.[14,38] To conduct the Förster resonance energy transfer (FRET) study, two lipophilic dyes were employed: 1,2-dioleoyl-*sn*-glycero-3-phosphoethanolamine-N-(lissamine rhodamine B sulfonyl) (DOPE-RhB, excitation/emission = 560/583 nm; Avanti Polar Lipids) and N-[6-[(7-nitro-2-1,3-benzoxadiazol-4-yl)amino]hexanoyl]-phytosphingosine (C6-NBD, excitation/emission = 460/534 nm; Avanti Polar Lipids). Both dyes were dissolved in chloroform and subsequently evaporated in a glass vial to form a thin film such that, with respect to platelet membrane protein, the final ratios would be 0.17 and 1.74 wt% for C6-NBD and DOPE-RhB, respectively. Solution containing platelet membrane was then added to the vial and stirred at 37 °C for 50 minutes. Afterwards, the free dye was washed away by centrifuging the membrane at 21,000 ×g for 15 minutes four times. RBC membrane was added to the DOPE-RhB/C-6NBD doped platelet membrane at RBC membrane to platelet membrane protein weight ratios of 5:1, 3:1, 2:1, 1:1, and 0:1, respectively, followed by stirring at 37 °C for 10 minutes to facilitate membrane fusion. The fluorescence spectrum of each sample was then read between 500 and 650 nm using an excitation wavelength of 470 nm on a Tecan Infinite M200 plate reader. Fluorescence recovery of the donor (C6-NBD) at the lower emission peak (534 nm) was used to indicate increasing amounts of fusion.

Nanoparticle Synthesis

Membrane-coated nanoparticles were fabricated by a previously reported sonication method.[14] Briefly, poly(lactic-*co*-glycolic acid) (PLGA) cores were fabricated using carboxylic acid-terminated PLGA polymer (0.67 dL/g, 50:50 ratio; Lactel Absorbable Polymers). The polymer was dissolved at 10 mg/mL in acetone and precipitated into water. Afterwards, the solution was placed under a vacuum aspirator until the organic solvent was removed. Either RBC membrane, platelet membrane, or fused RBC-platelet membrane at a 1:1 protein weight ratio was employed as the coating material. A mixture of PLGA cores and membrane material at a polymer to membrane protein weight ratio of 2:1 was then sonicated using a Fisher Scientific FS30D bath sonicator for 2 minutes to form the final coated nanoparticles.

Confocal Microscopy

To conduct the membrane colocalization study, RBC membrane was labeled with 1,1′-dioctadecyl-3,3,3′,3′- tetramethylindodicarbocyanine, 4-chlorobenzenesulfonate salt (DiD;

excitation/emission = 644/663 nm; Biotium) and platelet membrane with 5-(and 6)-carboxyfluorescein diacetate succinimidyl ester (CFSE, excitation/emission = 494/521 nm; eBiosciences). RBCNPs, PNPs, or [RBC-P]NPs made using these labeled membranes were then visualized under confocal fluorescence microscopy using an Olympus FV1000 microscope with a 100× oil objective. In order to obtain stable images, the particles were dispersed in glycerol to significantly decrease their mobility.

Membrane Loading

To assess the membrane loading ratio on [RBC-P]NPs, the nanoparticles were fabricated with DiD-labeled RBC membrane and CFSE-labeled platelet membrane at an input membrane protein weight ratio of 1:1. The nanoparticles were then centrifuged at 21,000 ×g to pellet the nanoparticles from the free membrane vesicles. The pelleted nanoparticles were resuspended back to their original volume. The fluorescence signal of each dye was measured before sonication and after resuspension using a Tecan Infinite M200 plate reader. For each dye, the data was normalized to the average signal obtained before sonication.

Physicochemical Characterization

Nanoparticle size and surface zeta potential were measured by dynamic light scattering (DLS) using a Malvern ZEN 3600 Zetasizer. The zeta potential of RBC, platelet, and fused membrane vesicles were also measured, giving values of approximately −25 mV in all cases. Transmission electron microscopy (TEM) was employed to visualize the nanoparticle structure. Samples were deposited on a glow-discharged, carbon-coated 400-mesh copper grid (Electron Microscopy Sciences). The grid was then washed using distilled water and negatively stained with vanadium (Abcam). Imaging was carried out on a Zeiss Libra 120 PLUS EF-TEM transmission electron microscope.

Stability Study

To evaluate the stability of the different nanoformulations in solution over time, bare PLGA cores, RBCNPs, PNPs, and [RBC-P]NPs were suspended in either water or 1× PBS (pH 7.4) at a final concentration of 1 mg/mL. At set timepoints over the course of 3 weeks, the sizes of the samples were measured by DLS to test for aggregation. To evaluate the stability in serum, a previously reported absorbance-based method was employed.[39] Nanoparticle samples were added to an equivalent volume of 2× fetal bovine serum (Hyclone) concentrated using 10 kDa MWCO Amicon centrifugal filters (EMD Millipore). The absorbance at 560 nm was measured, and the background signal from equivalent blank solutions was subtracted to give the reported values. Long-term stability was evaluated by measuring nanoparticle size before lyophilizing in 10 wt% sucrose solution using a Labconco FreeZone 4.5 L benchtop freeze dry system and after resuspension back to the original volume in water.

Protein Characterization

To examine the protein profile of RBCNPs, PNP, [RBC-P]NPs, and their corresponding membranes, SDS-PAGE was employed followed by incubation in InstantBlue Protein Stain (Expedeon). All samples were prepared in lithium dodecyl sulfate (LDS) sample loading

buffer (Invitrogen) and run at equivalent protein concentrations on NuPAGE Novex 4–12% Bis-Tris minigels (Invitrogen) in MOPS running buffer (Invitrogen). Western blotting was conducted to assess the presence of specific protein markers. Gels were transferred onto a nitrocellulose membranes (Thermo Scientific) and probed with antibodies specific for human CD41 (HIP8; Biolegend), CD47 (B6H12; eBiosciences), CD61 (VI-PL2; Biolegend), CD235a (HI264; Biolegend), and A antigen (HE-193; Abcam) along with the appropriate HRP-conjugated secondaries against mouse IgG (Biolegend) or mouse IgM (SouthernBiotech). To conduct the immunogold staining, samples were deposited on a glow-discharged, carbon-coated 400-mesh copper grid. The grid was then blocked with 5 wt% bovine serum albumin (BSA; Sigma Aldrich) in PBS, stained with a cocktail of mouse anti-human CD61 (VI-PL2; Biolegend) and rabbit anti-human CD235a (EPR8200; Abcam), washed with BSA solution, stained with a cocktail of gold-conjugated secondaries against mouse IgG (6 nm gold; Aurion) and rabbit IgG (15 nm gold; Aurion), washed with BSA solution, fixed with 1 wt% glutaraldehyde (Sigma Aldrich) in PBS, washed with distilled water, and stained with vanadium. Imaging was carried out on a Zeiss Libra 120 PLUS EF-TEM transmission electron microscope.

Macrophage Uptake Study

Human THP-1 cells (TIB-202; American Type Culture Collection) were maintained in RPMI 1640 (Life Technologies) supplemented with 10% FBS (Sigma Aldrich) and penicillin-streptomycin (Gibco). The cells were differentiated into a macrophage-like phenotype by incubating in 100 ng/mL phorbol myristate acetate (Sigma Aldrich) for 48 hours. Fluorescently labeled nanoparticles were fabricated by incorporating 0.1 wt% DiD into the PLGA cores during synthesis. The different nanoformulations were incubated with the cells at a final concentration of 0.25 mg/mL for 10 minutes at 37 °C. The media were then replaced with fresh media and the cells were incubated for another 30 minutes. Afterwards, the cells were washed 3 times with PBS and detached by scraping. Fluorescent signal was measured on a Becton Dickinson FACSCanto-II flow cytometer and analyzed using FlowJo software.

Cell-Specific Functional Study

As an RBC-specific property, the level of acetylcholinesterase in the different nanoformulations was assessed. Samples were analyzed using an Amplex Acetylcholine/Acetylcholinesterase Assay kit (Life Technologies) according to the manufacturer's instructions. To assess detoxification ability, 150 μL of the nanoformulations at 5 mg/mL was incubated with 5 μL of dichlorvos (Sigma Aldrich) solution at 10 μg/mL. Each sample was then centrifuged at 21,000 ×g to pellet the nanoparticles. The supernatant was analyzed by high performance liquid chromatography (HPLC) using a PerkinElmer Brownlee C18 analytical column (4.6 × 100 mm; 3 μm particle size) with a mobile phase of 50:50 water to acetonitrile, a flow rate of 1.0 mL/min, and a detector wavelength of 215 nm. The data was normalized using values obtained from a sample without nanoparticles.

As a platelet-specific property, the ability of the nanoformulations to bind metastatic cancer cells was assessed. Human MDA-MB-231 breast cancer cells (HTB-26; American Type Culture Collection) and HFF-1 foreskin fibroblasts (SCRC-1041; American Type Culture

Collection) were grown in DMEM (Corning) supplemented with FBS and penicillin-streptomycin. Nanoformulations with DiD-labeled PLGA cores were added to each well at a final concentration of 0.25 mg/mL and incubated for 5 minutes on ice to minimize cellular uptake. The cells were then washed 3 times with cold PBS and detached by scraping for flow cytometric analysis. Fluorescent signal was measured on a Becton Dickinson FACSCanto-II flow cytometer and analyzed using FlowJo software. For the fluorescent imaging, the cells were plated on 8-well Lab-Tek II chamber slides (Nunclon) and incubated with the nanoformulations as described above. In the co-culture study, HFF-1 cells were first labeled with CFSE and mixed with MDA-MB-231 cells at a 1:1 ratio. The cells were then fixed with 10% buffered formalin phosphate (Fisher Scientific), mounted with VECTASHIELD Antifade mounting media with DAPI (Vector Laboratories), and imaged on an Olympus FV1000 confocal microscope. Images were representative of the experiment done in triplicate and all were subjected to the same brightness and contrast adjustments. For in vivo targeting study, ApoE knockout mice (The Jackson Laboratory) were fed a high fat western diet to develop atherosclerosis. They were then administered 0.5 mg of DiD-labeled RBCNPs, [RBC-P]NPs, or PNPs. After 24 hours, the mice were euthanized, and the aortas isolated for imaging using a Keyence BZ-9000 fluorescence microscope. Oil Red O (Sigma Aldrich) staining was performed to confirm the presence of plaque via brightfield visualization. All animal experiments were performed in accordance with NIH guidelines and approved by the Institutional Animal Care and Use Committee (IACUC) of the University of California, San Diego.

In Vivo Characterization

Mouse RBCs and platelets were collected from 6-week-old male CD-1 mice (Harlan Laboratories) in order to fabricate mouse RBCNPs, PNPs, and [RBC-P]NPs. Fluorescently labeled nanoparticles were prepared using DiD-loaded PLGA cores. To perform the circulation study, 200 μL of fluorescently labeled particles at 3 mg/mL were administered intravenously. Blood was sampled by submandibular puncture at 3 minutes, 30 minutes, 1 hour, 3 hours, 7 hours, 24 hours, 48 hours, and 72 hours. Nanoparticle retention in circulation at these timepoints was determined by measuring the fluorescence on a Tecan Infinite M200 plate reader. The data from each mouse was normalized to the very first data point and analyzed using Graphpad Prism. Using a one-phase decay model, the half-lives were calculated from the fitted K parameter in the software as $t_{1/2} = \ln(2)/K$. The values of K with standard error for the RBCNPs, PNPs, and [RBC-P]NPs were 0.1213 ± 0.0182, 0.1219 ± 0.0240, and 0.1092 ± 0.0144 hr^{-1}, respectively. To calculate the two-phase elimination half-life, the normalized signal was transformed using natural log, and the slow phase from the resulting data was fitted using a linear regression curve. Elimination half-life was calculated as $t_{1/2} = \ln(2)/\beta$, where β is the negative slope obtained from the fit. The values of β with standard error for the RBCNPs, PNPs, and [RBC-P]NPs were 0.0164 ± 0.0045, 0.0181 ± 0.0042, and 0.0134 ± 0.0034 hr^{-1}, respectively. To study the biodistribution of the different nanoparticles, 200 μL of fluorescently labeled formulations at 3 mg/mL were administered intravenously. At 24 hours, mice were euthanized and perfused with 1× PBS. Afterwards, the heart, lungs, kidneys, liver, and spleen were collected and homogenized in 500 μL of water using a Biospec Mini-Beadbeater-16. Fluorescence was read using a Tecan Infinite M200 plate reader.

Acknowledgments

This work is supported by the National Institutes of Health under Award Numbers R01CA200574 and R01EY025947. We acknowledge the Waitt Advanced Biophotonics Core Facility of the Salk Institute for TEM imaging, which is supported with funding from NIH-NCI CCSG: P30 014195, NINDS Neuroscience Core Grant and the Waitt Foundation.

References

1. Hu CMJ, Fang RH, Luk BT, Zhang L. Nanoscale. 2014; 6:65. [PubMed: 24280870]
2. Farokhzad OC, Langer R. ACS Nano. 2009; 3:16. [PubMed: 19206243]
3. Allen TM, Cullis PR. Adv Drug Deliv Rev. 2013; 65:36. [PubMed: 23036225]
4. Gupta AK, Naregalkar RR, Vaidya VD, Gupta M. Nanomedicine. 2007; 2:23. [PubMed: 17716188]
5. Brannon-Peppas L, Blanchette JO. Adv Drug Deliv Rev. 2004; 56:1649. [PubMed: 15350294]
6. Wang AZ, Langer R, Farokhzad OC. Annu Rev Med. 2012; 63:185. [PubMed: 21888516]
7. Luk BT, Zhang L. ACS Appl Mater Interfaces. 2014; 6:21859. [PubMed: 25014486]
8. Luk BT, Fang RH, Zhang L. Theranostics. 2012; 2:1117. [PubMed: 23382770]
9. Pearce TR, Shroff K, Kokkoli E. Adv Mater. 2012; 24:3803. [PubMed: 22674563]
10. Kroll A, Fang RH, Zhang L. Bioconjug Chem. 2016; doi: 10.1021/acs.bioconjchem.6b00569
11. Luk BT, Zhang L. J Control Release. 2015; 220:600. [PubMed: 26210440]
12. Zhang P, Liu G, Chen X. Nano Today. 2016; doi: 10.1016/j.nantod.2016.10.008
13. Mitragotri S, Lahann J. Adv Mater. 2012; 24:3717. [PubMed: 22807037]
14. Hu CMJ, Fang RH, Wang KC, Luk BT, Thamphiwatana S, Dehaini D, Nguyen P, Angsantikul P, Wen CH, Kroll AV, Carpenter C, Ramesh M, Qu V, Patel SH, Zhu J, Shi W, Hofman FM, Chen TC, Gao W, Zhang K, Chien S, Zhang L. Nature. 2015; 526:118. [PubMed: 26374997]
15. Gao W, Zhang L. AIChE J. 2015; 61:738.
16. Hu Q, Qian C, Sun W, Wang J, Chen Z, Bomba HN, Xin H, Shen Q, Gu Z. Adv Mater. 2016; 28:9573. [PubMed: 27626769]
17. Balmert SC, Little SR. Adv Mater. 2012; 24:3757. [PubMed: 22528985]
18. Fang RH, Hu C-MJ, Luk BT, Gao W, Copp JA, Tai Y, O'Connor DE, Zhang L. Nano Lett. 2014; 14:2181. [PubMed: 24673373]
19. Rao L, Bu LL, Cai B, Xu JH, Li A, Zhang WF, Sun ZJ, Guo SS, Liu W, Wang TH, Zhao XZ. Adv Mater. 2016; 28:3460. [PubMed: 26970518]
20. Sun H, Su J, Meng Q, Yin Q, Chen L, Gu W, Zhang P, Zhang Z, Yu H, Wang S, Li Y. Adv Mater. 2016; 28:9581. [PubMed: 27628433]
21. Hu CMJ, Zhang L, Aryal S, Cheung C, Fang RH, Zhang L. Proc Natl Acad Sci U S A. 2011; 108:10980. [PubMed: 21690347]
22. Hu CMJ, Fang RH, Luk BT, Chen KNH, Carpenter C, Gao W, Zhang K, Zhang L. Nanoscale. 2013; 5:2664. [PubMed: 23462967]
23. Hu CMJ, Fang RH, Copp J, Luk BT, Zhang L. Nat Nanotechnol. 2013; 8:336. [PubMed: 23584215]
24. Hu CMJ, Fang RH, Luk BT, Zhang L. Nat Nanotechnol. 2013; 8:933. [PubMed: 24292514]
25. Pang Z, Hu CMJ, Fang RH, Luk BT, Gao W, Wang F, Chuluun E, Angsantikul P, Thamphiwatana S, Lu W, Jiang X, Zhang L. ACS Nano. 2015; 9:6450. [PubMed: 26053868]
26. Wang F, Gao W, Thamphiwatana S, Luk BT, Angsantikul P, Zhang Q, Hu CMJ, Fang RH, Copp JA, Pornpattananangkul D, Lu W, Zhang L. Adv Mater. 2015; 27:3437. [PubMed: 25931231]
27. Gao W, Fang RH, Thamphiwatana S, Luk BT, Li J, Angsantikul P, Zhang Q, Hu CMJ, Zhang L. Nano Lett. 2015; 15:1403. [PubMed: 25615236]
28. Parodi A, Quattrocchi N, van de Ven AL, Chiappini C, Evangelopoulos M, Martinez JO, Brown BS, Khaled SZ, Yazdi IK, Enzo MV, Isenhart L, Ferrari M, Tasciotti E. Nat Nanotechnol. 2013; 8:61. [PubMed: 23241654]
29. Gao C, Lin Z, Jurado-Sánchez B, Lin X, Wu Z, He Q. Small. 2016; 12:4056. [PubMed: 27337109]

30. Dehaini D, Fang RH, Zhang L. Bioeng Transl Med. 2016; 1:30.
31. Fang RH, Hu CMJ, Chen KNH, Luk BT, Carpenter CW, Gao W, Li S, Zhang DE, Lu W, Zhang L. Nanoscale. 2013; 5:8884. [PubMed: 23907698]
32. Gagneux P, Varki A. Glycobiology. 1999; 9:747. [PubMed: 10406840]
33. Ma YQ, Qin J, Plow EF. J Thromb Haemost. 2007; 5:1345. [PubMed: 17635696]
34. Oldenborg PA, Zheleznyak A, Fang YF, Lagenaur CF, Gresham HD, Lindberg FP. Science. 2000; 288:2051. [PubMed: 10856220]
35. Rodriguez PL, Harada T, Christian DA, Pantano DA, Tsai RK, Discher DE. Science. 2013; 339:971. [PubMed: 23430657]
36. Gao W, Hu CMJ, Fang RH, Luk BT, Su J, Zhang L. Adv Mater. 2013; 25:3549. [PubMed: 23712782]
37. Hu Q, Sun W, Qian C, Wang C, Bomba HN, Gu Z. Adv Mater. 2015; 27:7043. [PubMed: 26416431]
38. Copp JA, Fang RH, Luk BT, Hu CMJ, Gao W, Zhang K, Zhang L. Proc Natl Acad Sci U S A. 2014; 111:13481. [PubMed: 25197051]
39. Fang RH, Aryal S, Hu CMJ, Zhang L. Langmuir. 2010; 26:16958. [PubMed: 20961057]

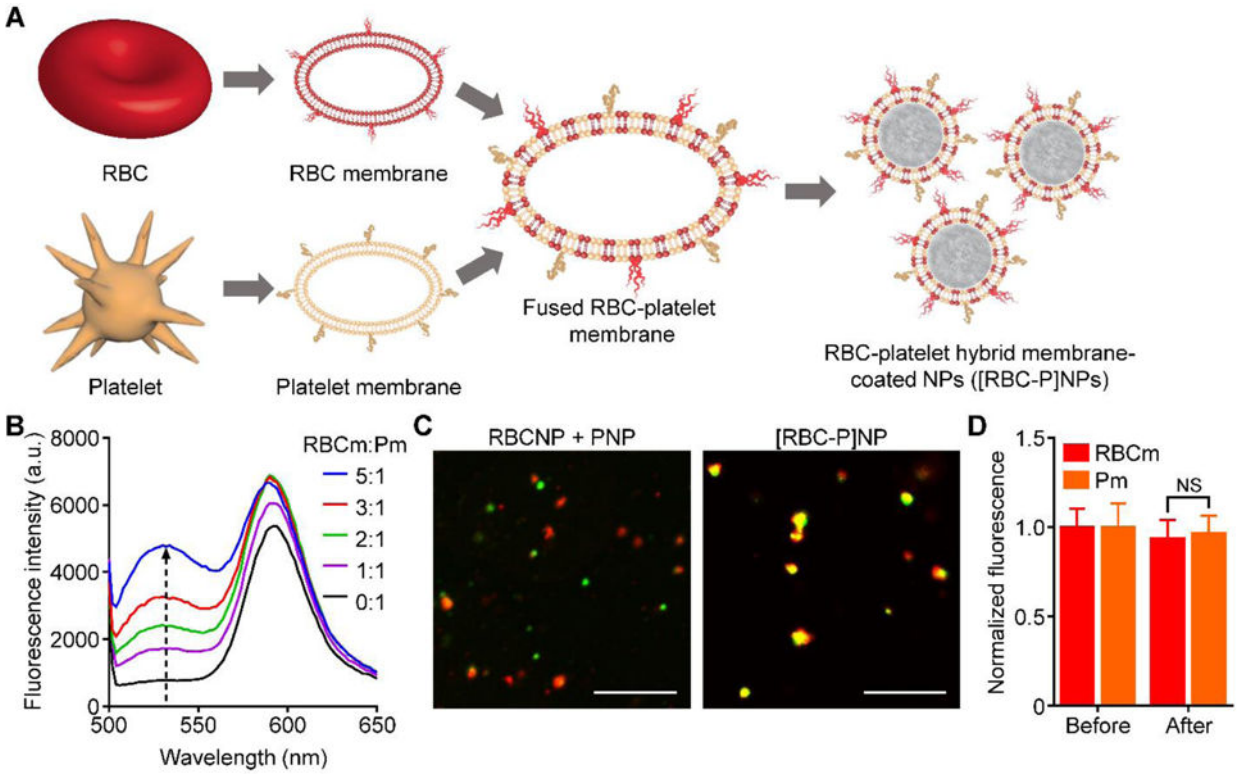

Figure 1.

Fabrication of RBC-platelet hybrid membrane-coated nanoparticles (denoted [RBC-P]NPs). A) Schematic of membrane fusion and coating. Membrane material is derived from both RBCs and platelets and then fused together. The resulting fused membrane is used to coat poly(lactic-*co*-glycolic acid) (PLGA) polymeric cores to produce [RBC-P]NPs. B) Platelet membrane was doped with a FRET pair of fluorescent probes and mixed with increasing amounts of RBC membrane. The recovery of the fluorescence emission from the donor at the lower emission peak (534 nm) was monitored (RBCm:Pm = RBC membrane to platelet membrane protein ratio). C) Confocal fluorescent microscopy images of either a mixture of RBCNPs and PNPs or of the [RBC-P]NPs (red = RBC membrane, green = platelet membrane; scale bar = 10 μm). D) Fluorescent quantification of dye-labeled RBCm and Pm inputted to [RBC-P]NPs at a 1:1 protein ratio before the coating process and after purification of the coated nanoparticles (n = 3; mean ± SD). For each type of membrane, the data was normalized to the before values. NS = not significant, Student's *t*-test.

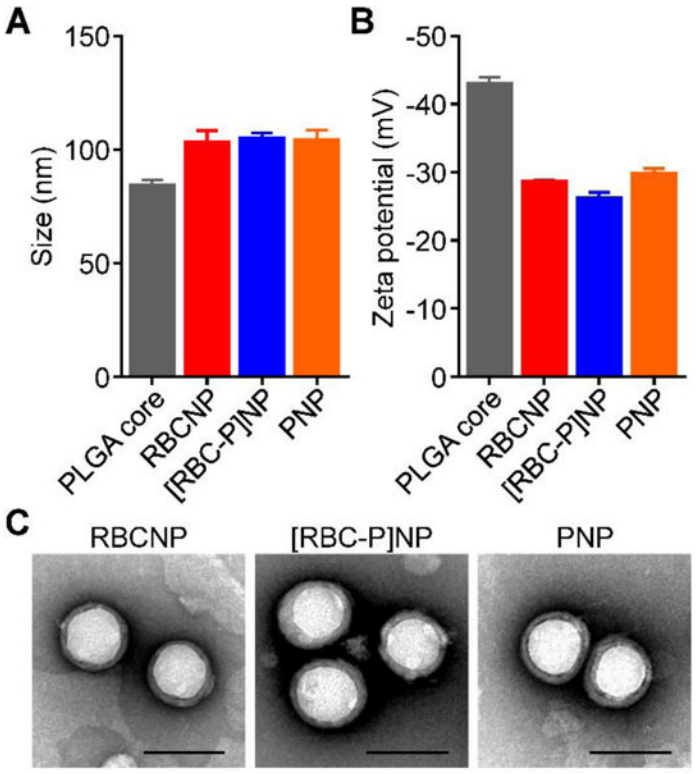

Figure 2.

Physicochemical characterization. A) Z-average size of bare PLGA cores, RBCNPs, [RBC-P]NPs, and PNPs as measured by DLS (n = 3; mean ± SD). B) Surface zeta potential of bare PLGA cores, RBCNPs, [RBC-P]NPs, and PNPs as measured by DLS (n = 3; mean ± SD). C) Representative TEM images of RBCNPs, [RBC-P]NPs, and PNPs negatively stained with vanadium (scale bar = 100 nm).

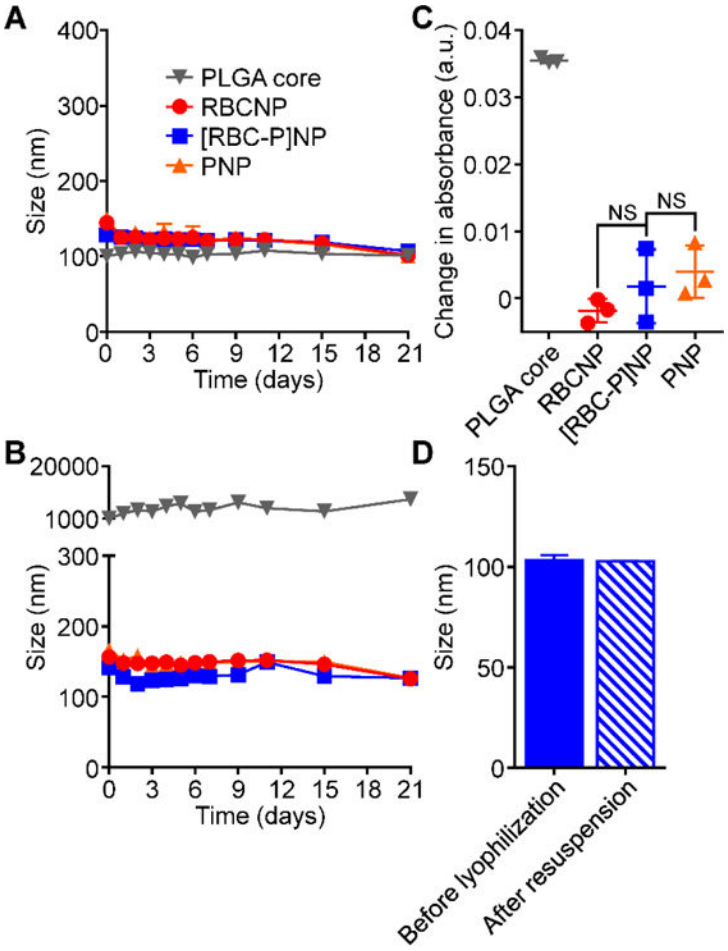

Figure 3.

Nanoparticle stability. A) Z-average size of bare PLGA cores, RBCNPs, [RBC-P]NPs, and PNPs over 3 weeks in water (n = 3; mean ± SD). B) Z-average size of bare PLGA cores, RBCNPs, [RBC-P]NPs, and PNPs over 3 weeks in PBS (n = 3; mean ± SD). C) Change in absorbance at 560 nm of PLGA cores, RBCNPs, [RBC-P]NPs, and PNPs after transferring into 100% serum from water. An increase in absorbance was used to indicate particle aggregation. NS = not significant, Student's *t*-test. D) Z-average size of [RBC-P]NPs before lyophilization in 10 wt% sucrose and after resuspension (n = 3; mean ± SD).

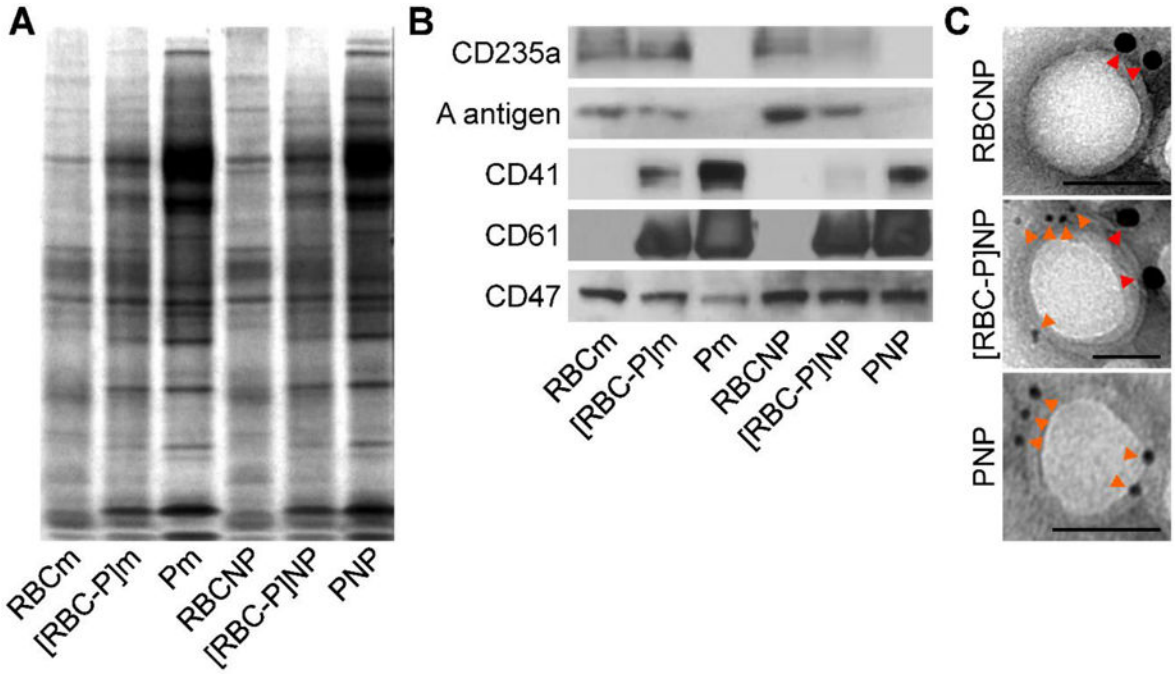

Figure 4.

Protein characterization. A) Protein content visualization of RBC membrane (RBCm), fused RBC-platelet membrane ([RBC-P]m), platelet membrane (Pm), RBCNPs, [RBC-P]NPs, and PNPs run on SDS-PAGE at equivalent protein concentrations followed by Coomassie staining. B) Western blot analysis of RBCm, [RBC-P]m, Pm, RBCNPs, [RBC-P]NPs, and PNPs for characteristic RBC markers CD235a (glycophorin A) and A antigen, characteristic platelet markers CD41 (integrin αIIb) and CD61 (integrin β3), and a shared marker CD47. All samples were run at equivalent protein concentrations. C) Immunogold TEM images of RBCNP, [RBC-P]NP, and PNP samples probed for CD235a (red arrows, large gold) and CD61 (orange arrows, small gold) followed by negative staining with vanadium (scale bars = 50 nm).

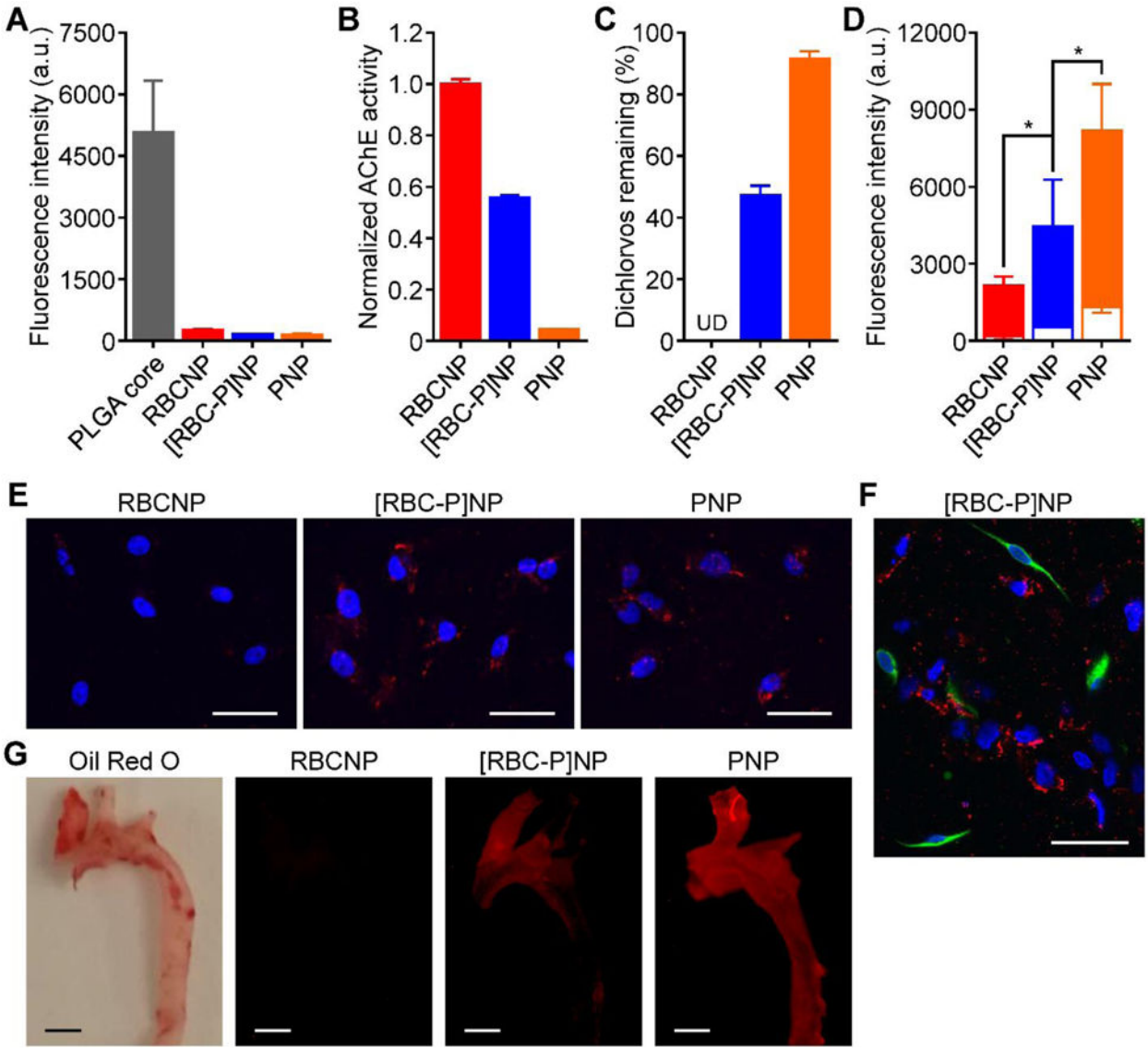

Figure 5.

Membrane biological function assays. A) Uptake of fluorescently labeled bare PLGA cores, RBCNPs, [RBC-P]NPs, and PNPs when incubated with human macrophage-like cells as analyzed by flow cytometry (n = 3; mean ± SD). B) Acetylcholinesterase activity of RBCNPs, [RBC-P]NPs, and PNPs measured by an Amplex acetylcholinesterase assay kit (n = 3; mean ± SD). C) Amount of free dichlorvos, a model organophosphate, remaining in solution after incubation with RBCNPs, [RBC-P]NPs, or PNPs (n = 3; mean ± SD). UD = undetectable. D) Binding of fluorescently labeled RBCNPs, [RBC-P]NPs, and PNPs to human MDA-MB-231 breast cancer cells (solid bars) or human HFF-1 foreskin fibroblasts (open bar overlays) as analyzed by flow cytometry (n = 3; mean ± SD). $^{*}P < 0.05$, one-tailed Student's *t*-test. E) Confocal fluorescence imaging of dye-labeled RBCNPs, [RBC-P]NPs, and PNPs after incubation with MDA-MB-231 cells (red = nanoparticles, blue = nuclei; scale bars = 50 μm). F) Confocal fluorescence imaging of dye-labeled [RBC-P]NPs after incubation with a co-culture of MDA-MB-231 and HFF-1 cells (red = nanoparticles, green =

HFF-1 membrane, blue = nuclei; scale bar = 50 μm). G) Imaging of aortas from ApoE knockout mice fed with a high fat western diet after intravenous administration with dye-labeled RBCNPs, [RBC-P]NPs, and PNPs (red = nanoparticles; scale bars = 1 mm). Oil Red O staining was used to confirm the presence of atherosclerotic plaque.

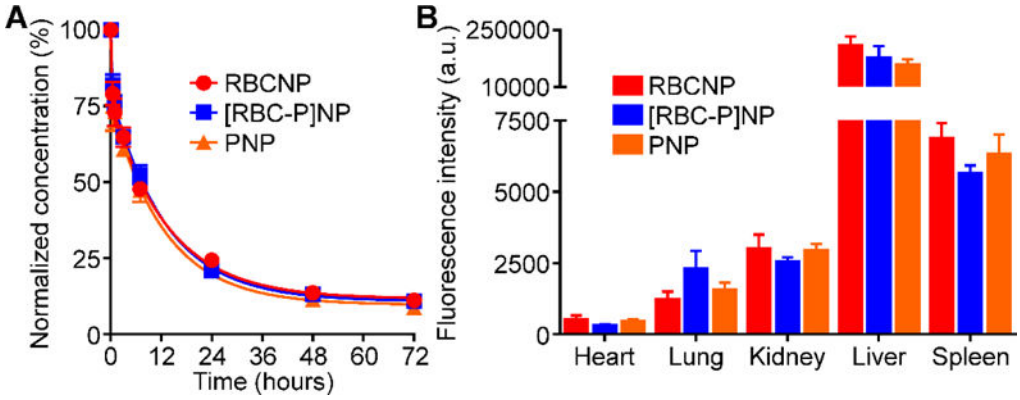

Figure 6.

In vivo characterization. A) Circulation time of fluorescently labeled RBCNPs, [RBC-P]NPs, and PNPs after intravenous administration to mice via the tail vein (n = 4; mean ± SEM; lines represent two-phase decay model). B) Biodistribution of fluorescently labeled RBCNPs, [RBC-P]NPs, and PNPs 24 hours after intravenous administration to mice via the tail vein (n = 4; mean ± SEM).